Chapter

High-Wavenumber Raman Analysis

Shan Yang

Abstract

Raman spectra are molecule specific, and their peaks in the fingerprint region (200-2000 cm^{-1}) are often sufficient for material identification. High-wavenumber signals (> 2000 cm^{-1}) are rare in inorganic material but rich in organic materials containing light hydrogen atoms. Reports on high-wavenumber (HW) Raman signals are far less than fingerprint signals. This could be partially attributed to the difficulty obtaining HW Raman signals, especially from biological materials containing fluorescent proteins. The development and the availability of InGaAs array and the near-infrared (NIR) laser enabled the acquisition of distinct HW Raman from bio-materials. In this chapter, we will introduce recent applications of HW Raman spectroscopy on different materials, especially on biological tissues. Raman instrumentation based on multiple lasers or multiple spectrometers will also be discussed.

Keywords: High-wavenumber Raman, High-fluorescent, Dental Hard tissues, Hydration, Water analysis

1. Introduction

Raman scattering is the inelastic scattering of photons by a matter; specifically, it results from the interactions between the photons and molecular vibrations in the matter. In a simple scenario, a molecule is composed of two atoms, and the vibrational energy of such a diatomic molecule can be approximately treated as a simple harmonic oscillator with the energy states of $E_n = \frac{\left(n+\frac{1}{2}\right)h}{2\pi}\sqrt{\frac{k}{\mu}}$, where n is the vibrational quantum number that can take values of 0, 1, 2, and so on; k is a spring constant, and $\mu = \frac{m_1 m_2}{m_1 + m_2}$ is the reduced mass of the two atoms. This approximation indicates the vibrational energy inversely proportional to the square root of the reduced mass. Therefore, diatomic molecules composed of light atoms have higher vibration energies; in other words, their Raman signals appear at higher wavenumber regions than those consisting of heavier atoms. For complex molecules composed of multiple atoms, a bond connecting two atoms will be influenced by other atoms nearby; however, bonds connecting lighter atoms still yield Raman signals at higher wavenumber regions in general. **Table 1** shows Raman signal positions of several common molecules and chemical bonds [1, 2].

Molecules or chemical bonds	Vibration modes	Raman frequency [cm^{-1}]
H_2	stretch	4395
H_2O	symmetric stretch	3657
CO	stretch	2170
HCl	stretch	2990
NO	stretch	1904
OH of hydroxyapatite	OH stretch	3570
PO_4 of hydroxyapatite	symmetric stretch	960
CH of CH4	symmetric stretch	2914

Table 1.
Raman frequencies of representative molecules and chemical bonds.

Detection of high-wavenumber (HW) Raman signals is as simple as other Raman signals for most of the inorganic materials (e.g., water, graphene) and nonliving organic material (e.g., alcohol, glycerol etc.). However, obtaining HWRaman signals from biological tissues, which have auto-fluorescent emissions under laser excitation, has been challenging. As an inelastic scattering, the Raman effect can happen with lasers at any wavelength from UV lights to near-infrared. However, excitation with lasers at a shorter wavelength is preferred because the efficiency of Raman scattering is inversely proportional to the fourth-order of the incident wavelength. Reduce the excitation, e.g., by a factor of 2, could easily lead to the increase of signal intensity by a factor of 16, which is significant to most Raman studies with low scattering efficiency (in the order of one part per million) [3]. On the other hand, the higher energy photons of the shorter wavelength are more capable of producing fluorescence from materials (especially biological tissues) which could overwhelm the weak Raman signals of interests [4]. Excitation with lasers at longer wavelength has been shown to be a major practice that could alleviate the strong fluorescence from biological tissues [5]. Therefore, for a given material with high auto-fluorescence, exploring various excitation wavelengths may be employed to find the optimal one [6–10].

In addition to the need to balance lower fluorescence interference and higher collecting efficiency, several factors in Raman instrumentations (e.g., the availability of lasers and detectors) should also be considered for detecting HWRaman signals. The most critical component in Raman instrumentation is the Raman spectrometer, which varies from simple, compact version to user-adjustable complex version. Research grade Raman spectrometers allow users to modify componential configurations such as replacing detectors, changing gratings, adjusting slit width, repositioning focusing mirror, etc. The combination of small slit width, high groove density grating, and long focal distance can allow research-grade spectrometers to achieve sub-wavenumber (cm^{-1}) spectral resolution [11]. Compact Raman spectrometers have fixed spectral range and resolution and usually allow none/limited configuration modifications for end users. However, utilizing high-dispersion and high-efficiency volume phase transmission gratings, as well as sensitivity enhancement (through back illumination and special coating) and noise reduction (through one or two stages of thermal electric cooling), the compact spectrometers can achieve comparable and even higher signal to noise ratio than research-grade spectrometers under similar experiment conditions (e.g., laser power, integration time, and spectral resolution). In addition, having no moving parts in the device, compact spectrometers are generally robust and appropriate for fieldwork or on-site tasks.

The small dimension of the detector sensor/chip determines that the spectral resolution must compromise with the covered spectral range, especially for compact

spectrometers. Most commercial compact Raman spectrometers can only cover ~200-2000 cm^{-1} with a resolution in the range of 6-12 cm^{-1}. Majority of modern Raman spectrometers are based on silicon-based CCD detectors, which usually have optimal responses between 400 and 900 nm. Although this range may be slightly extended through UV or NIR enhanced technologies [12–15], CCD-detector based UV and NIR Raman studies out the range of 400-900 nm are scarce. As the result of the consideration of factors mentioned above, i.e., the need to balance Raman efficiency and autofluorescence and the availability of lasers and detectors, the combination of the 785 nm laser excitation and a NIR enhanced CCD detector has been chosen for most biologically related Raman studies. The results turned out to be satisfactory in many cases, especially signals in the fingerprint region (i.e., 200 – 2000 cm^{-1}).

The high-wavelength Raman signals from chemical bonds involving hydrogen atoms (e.g., CH and OH) will appear above 2900 cm^{-1} (see **Table 1**). With NIR enhanced silicon-based CCD detector, the CH groups appearing near 2900 cm^{-1} may be weakly observed, but the OH related signal expecting near 3500 cm^{-1} (corresponding to ~1090 nm) is hardly observable. Earlier literature reports on HW Raman signals from biological samples seemed primarily conducted by Fourier Transformed Raman spectroscopy (FT-Raman) [16–19]. FT-Raman is typically composed of Nd:Yag laser and germanium detector, it ghus has the great adavantages of fluorescence reduction and high resulution. However, because all the lights including the residuals of the laser simultaneously strikes the detector, FT-Raman is detector noise limited and typically requires much longer (up to 3 orders) integration time than dispersive Raman system [19, 20]. This explained why FT-Raman is still not very popular despite it has emerged over three decades.

Indium gallium arsenide (InGaAs) based arrays have emerged as a dispersive detector for spectroscopy devices around 2000 [21]. Unlike CCD, InGaAs has optimal sensitivity across 900-1700 nm, and has gained increasing interest for Raman applications based on 1064 nm laser as its great potential in further suppress the auto-fluorescence, especially from biological tissues. Unal et al. demonstrated that the InGaAs spectrometer designated for 1064 nm Raman spectroscopy can be combined with 852 nm laser to probe hydrations in bone tissues [22]. Yang and He et al. modified the system with a 866 nm laser and demonstrated water detection in other biological tissues, including animal skin, human teeth, and fruits [23–25]. For example, the Raman spectrum acquired with an InGaAs Raman spectrometer under 866/1064 nm dual excitation (red curve) shows strong signals from CH and OH bonds. Those signals were barely observable with Raman spectroscopy composing a 785 nm laser and a CCD detector (**Figure 1**).

2. HW Raman of non-living matters

Room temperature HW Raman signals typically result from chemical bonds formed by light atoms such as CO, CH, OH, CN. In contrast, the signals greater than 2500 cm^{-1} mostly result from chemical bonds containing hydrogen atoms (e.g., CH and OH groups), except for second-order processes, e.g., the 2D signal in graphene. HW Raman signals of the majority of inorganic compounds and non-living organic materials can be illuminated with visible light (e.g., 532 nm or 633 nm) without exciting problematic fluorescence interference. For example, Raman signals from water can be acquired with Raman spectroscopy at any wavelengths from UV to NIR as long as the detector responds. The HW Raman signals from hydroxyapatite crystal, the primary component in human mineral tissues, can also be obtained under the illumination of a green laser at 515 nm [2].

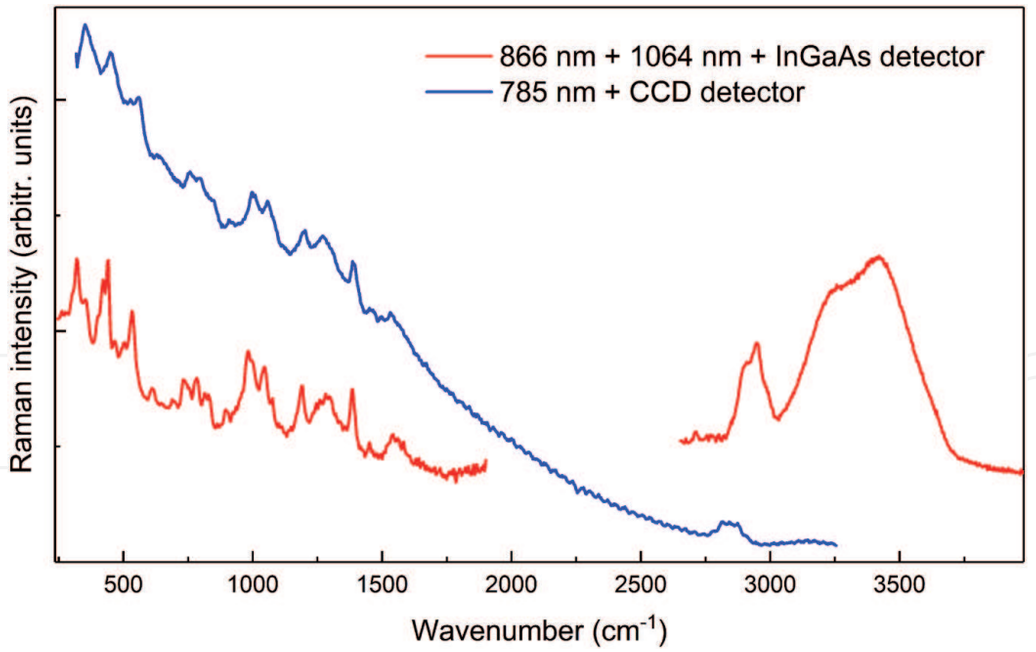

Figure 1.
Raman spectra of grape skin acquired with 785 nm (blue curve) excitation and CCD.

Simple and small molecule organic materials with a low visible light absorption rate can generally be examined with visible Raman spectroscopy. Thus their full range Raman spectra covering the HW Raman signals can be acquired as easily as fingerprint signals. Despite the fingerprint Raman signals of these material are sufficient for identification, HW Raman signals can provide additional information to understand the molecular dynamics. Nedić et al. studied water, methanol, ethanol dimer and trimers and found that both methanol and ethanol are better hydrogen bond donors and acceptors than water through investigating the red shif of HW OH signals [26]. In addition, Starciuc et al. were able to study the tranisitions of unclusered water to large water clusters through the analysis of highwavenumber and lowwave number Rmaan signals in mixed glycerol-water system [27].

3. HW Raman analysis on biological tissues using CCD detectors

Although the HW region Raman signals, including CH, NH, and OH bonds, are informative in analyzing biological tissues, as seen in many Fourier Transformed Infrared (FTIR) absorption spectrum, Raman studies in this region on biological tissues have been underperformed. Other than the few studies using FT-Raman spectrometer, there are several studies using CCD-based dispersive Raman spectrometers. Santos et al. investigated the effects of different optical fibers on 720 nm laser based Raman spectroscopy and demonstrated the system was capable of acquireing HW Ramang signals from sliced porce brain tissues [28]. Carvalho et al. demonstrated HW Raman signals may be obtained with 532 nm laser from oral cells immersed in distilled water [29]. Barroso et al. studied the difference of HW Raman signals between healthy and cancer oral tissues and found that water contents may be used as a biomarker for cancer diagnosis [30]. It is worth to note that all these biological tissues that was able to stuied by the visible light do not produce intense fluorescence that overwhelm the Raman signals. Skin tissue is also one type of tisse that does not have problematic fluorescenc under Raman study. Therefore, skin tissues especially the stratum corneum, have also been well studied in terms of HW Raman region. By using a confocal Raman micro-spectrometer to exclude out of plane fluorescence

DOI: http://dx.doi.org/10.5772/intechopen.100474

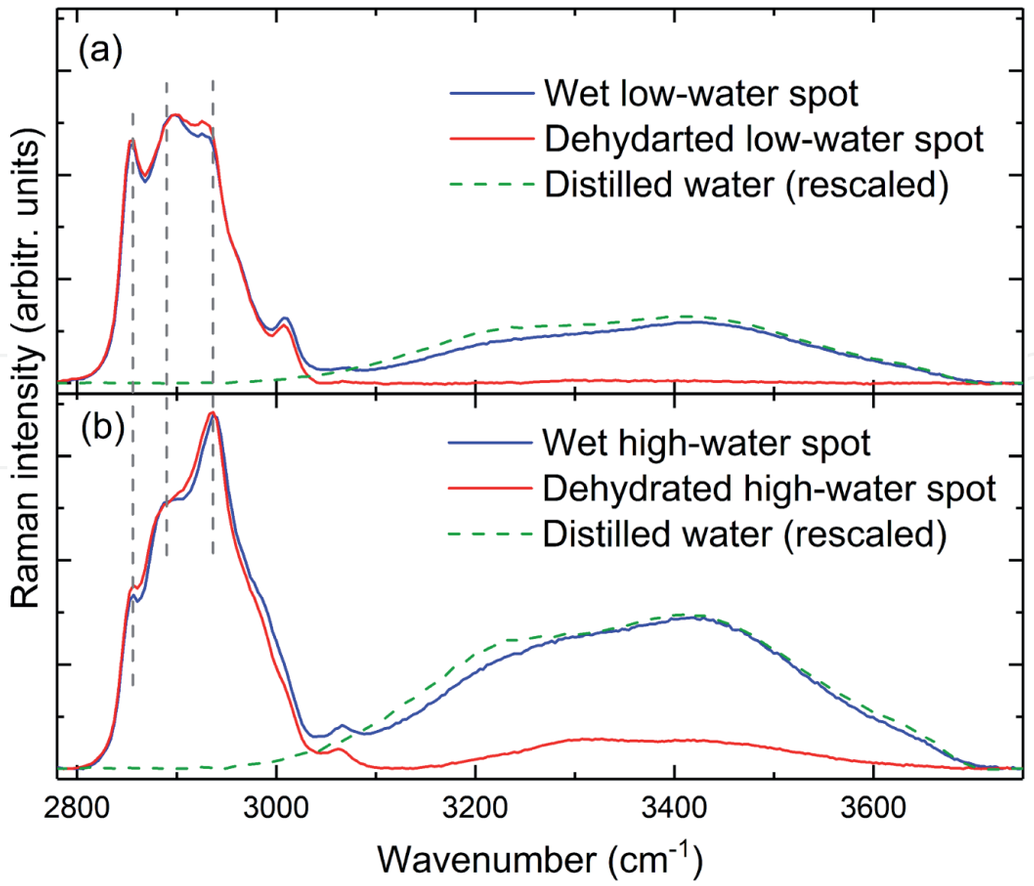

Figure 2.
Raman spectra of chicken skin at representative (a) low-water spots and (b) high-water spots before (blue curve) and after 24-hour air drying (red curve). Peaks marked with vertical dashed lines from low to high were located at 2854, 2895, and 2934 cm^{-1} respectively. The spectra were acquired with 85 mw, 866 nm laser light with 30 s exposure and 6 averages. All skin spectra were normalized according to the 2895 cm^{-1} signal for easier comparison, while the spectrum of distilled water was rescaled to match the corresponding OH signal of the skin.

emissions, the HW regions Raman signals were able to be acquired from human skins. Caspers et al. used a confocal Raman micro-spectrometer based on 720 nm excitation to obtain Raman spectra of skin showing clear water profile and detailed CH structures [31, 32]. Later, Choe et al. deconvoluted the CH and OH groups of Raman signal and studied the profile variation of bound water affected by protein and lipids interactions at different depths [33]; while Quatela et al. observed variation of spectral markers including OH and CH groups among different individuals [34]. It is worth noting that in Choe's work, two lasers operating at 671 nm and 785 nm were used. Such a dual-wavelength Raman setup is an alternative approach to acquiring the HW Raman signals when only a compact spectrometer with a fixed spectral range is available. For a compact Raman system designed for acquiring fingerprint region ~240-2000 cm^{-1} (corresponding to 800-930 nm) under 785 nm excitation, send in a second laser beam operating at 671 nm will effectively extend the spectral range to cover the region of ~2400-4100 cm^{-1} which include the main HW CH and OH groups.

In contrast to the study on the HW region Raman spectral variations with the depth of the skin tissue, Yang et al. investigated the lateral variations on the skin surface [25]. The team identified mainly two types of spots on the skin surface, i.e., high-water spots and low-water spots (**Figure 2**). Further analysis on other tissues, including muscle, fat, and tendons, the authors found that the skin tissues contain both fat and protein (keratin) and suggested the high-water spots on chicken skin are protein-rich while the low-water spots are lipids-rich. This suggestion is supported by the observation of the characteristic CH bonds (**Figure 3**) among these

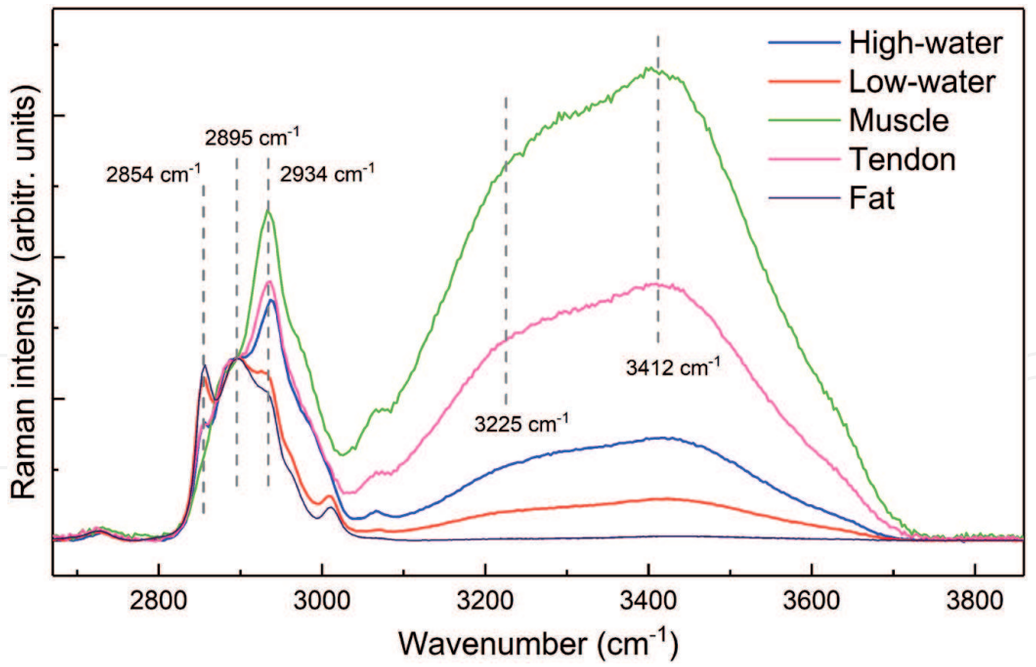

Figure 3.
Raman spectra of chicken tissues (a) before and (b) after dehydration (except fat). Spectra in (b) were vertically enlarged. Dehydrated fat was prepared with 6 hours of air drying at room temperature, while dehydrated muscle or tendon were prepared with 72 hours of air drying at room temperature or overnight oven drying at 45°C. All spectra were acquired under the condition of 85 mW laser at 866 nm illumination, with 30 s exposure, and averaged 6 times. All spectra in (a) and (b) were normalized according to the 2895 cm^{-1} signal.

tissues and the fact that the muscle tissue has the highest OH (3412 cm^{-1}) to CH (2895 cm^{-1}) signal intensity ratio, while the fat tissue has the lowest one among those tissues under investigation. Additional investigations on dehydrated tissues indicated that protein-rich tissues were more capable of retaining water and more resistant to dehydration. In other words, the protein component is positively correlated with skin hydration, in contrast to the fat component.

4. Water contents in mineral tissues

As mentioned earlier, the combination of the NIR laser lights near 850 nm and the InGaAs detector-based spectrometer allowed the observation of water contents in mineral tissues, including dental hard tissues and bones [22, 23]. Mineral tissues appeared more fluorescent than stratum corneum, and were challenging for Raman measurement using visible lights. Unal et al. characterized several HW peaks, including CH group and OH group, and suggest bound water in bone could be interacting with both collagen and mineral matrix [22]. He et al. discovered similar HW Raman signals from dental hard tissues, including dentin and enamel [23]. The authors demonstrated the spectral profile not only varied between enamel and dentin tissues but also varied among different locations within enamel tissues. As shown in **Figure 4**, representative spectra from dentin and enamel were stacked for comparison (rescaled Raman spectrum of distilled water was also provided for reference). The spectra were taken from the sagittal surface. The lower wavenumber region containing the fingerprint 960 cm^{-1} signal was acquired under 1064 nm laser excitation, while the HW region was acquired under 866 nm laser excitation. The spectra were normalized according to the 960 cm^{-1} signal intensity, and the same factor was applied to the HW region for consistency. The differences between the spectra indicated that both enamel and dentin contain water that is not 'free' like in

DOI: http://dx.doi.org/10.5772/intechopen.100474

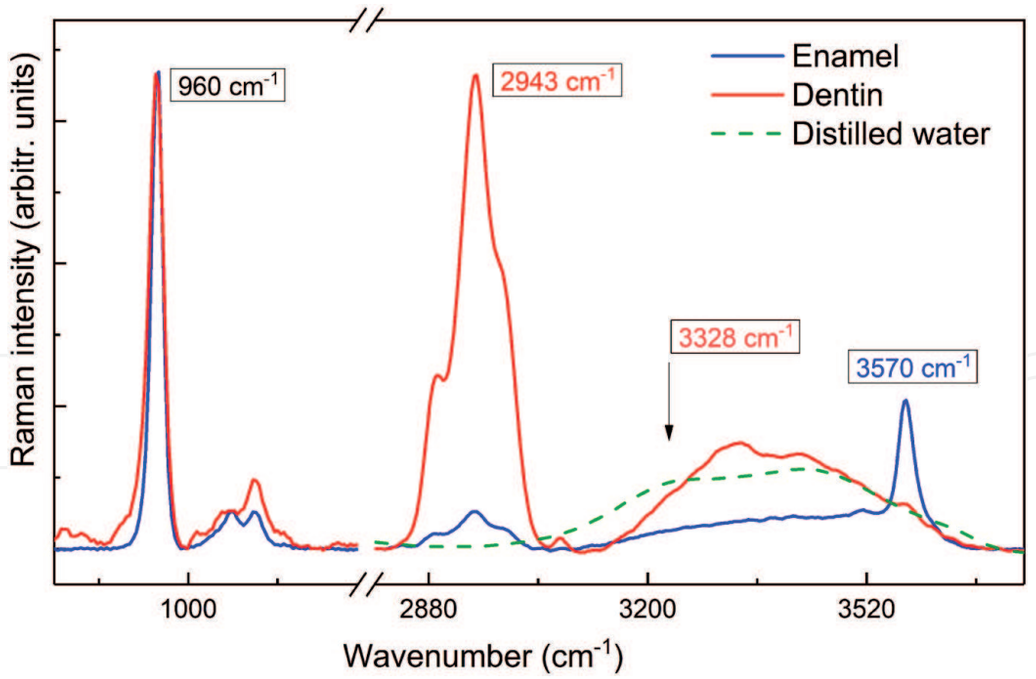

Figure 4.
Representative Raman spectra from enamel (blue curve) and dentin (red curve) portions from the sagittal surface of a tooth. Spectra below 1200 cm^{-1} were acquired under 20s 1064 nm excitation while the spectra above 3000 cm^{-1} were acquired under (30s × 16) 866 nm excitation. Water spectrum was scaled down for easier comparison.

distilled water, and dentin contains a greater number of organic components than enamel, evidenced by the much greater C-H stretch peak located at 2943 cm^{-1}. The author suggested part of the water in dentin interacts with the surrounding environment, likely the organic matrix, evidenced by the appearance of an additional peak at 3328 cm^{-1}, which could be partially contributed by the N-H bond (but not all considering its intensity) [35].

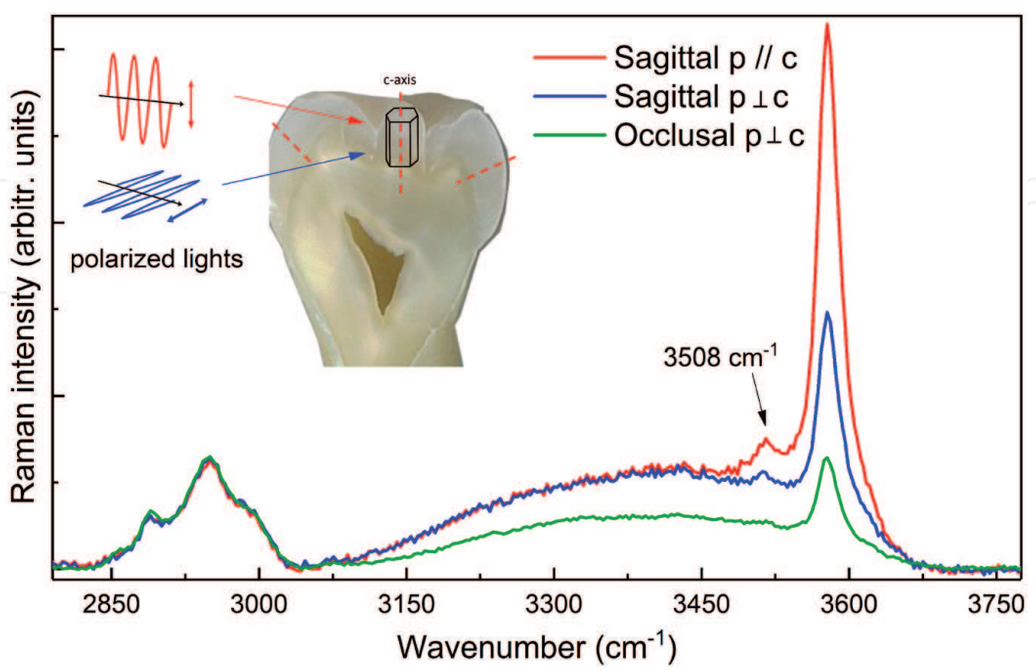

Figure 5.
Representative HW Raman spectra under linearly polarized laser excitation from internal and external surfaces of a tooth enamel. The inset shows the picture of the sagittal surface of a tooth, with dashed red line showing the approximate c-axis of HAP crystals of enamel layer. Experimental conditions are 30s × 16 integration time and 50 mW, 866 nm laser light illumination.

Another major difference between the enamel and dentin spectra is the appearance of a sharp 3570 cm^{-1} Raman signal in enamel, but the same signal is barely noticeable in dentin. Additional spectra acquired from different spots on enamel showed that the signal varied with locations (**Figure 5**). Further, the signal intensity from the same spot will also change with the polarization of the incident light. Because a very similar signal appears in synthetic hydroxyapatite crystals, the authors assign the peak at 3570 cm^{-1} to the OH radicals of hydroxyapatite crystals. This signal is polarization-dependent because most of the hydroxyapatite crystals align along the c-axis (see dashed red line in the inset tooth picture), which is roughly perpendicular to the external enamel surface. The difference in the signal between enamel and dentin tissues is mainly due to the sizes of hydroxyapatite crystals. The signal is stronger from internal enamel spots than external spots because the internal tissues keep better integrity.

The spectrum of enamel also showed a small difference between the internal and the external spots on enamel: a peak located at 3508 cm^{-1} that only obviously appearing in the spectra from internal enamel spots. This signal is absent in the spectra of single hydroxyapatite crystals or any hydroxyapatite powders reported before. Based on its similar location as the 3570 cm^{-1} signals this signal is suggested to be structure water bound to the mineral matrix of unaffected enamel tissue. In other words, this signal is likely the water that is bound to hydroxyapatite crystal, similar to how the OH radical forms during the crystal growth. The enamel may lose these bound waters when demineralization happens to the surface enamel.

5. HW Raman detection on pigmented biological materials

Pigmented tissues, from both animals and plants, are usually high fluorescent for Raman studies; thus, probing HW Raman signals from these tissues are difficult with visible lights. Muscle tissues showing in the previous section are one example

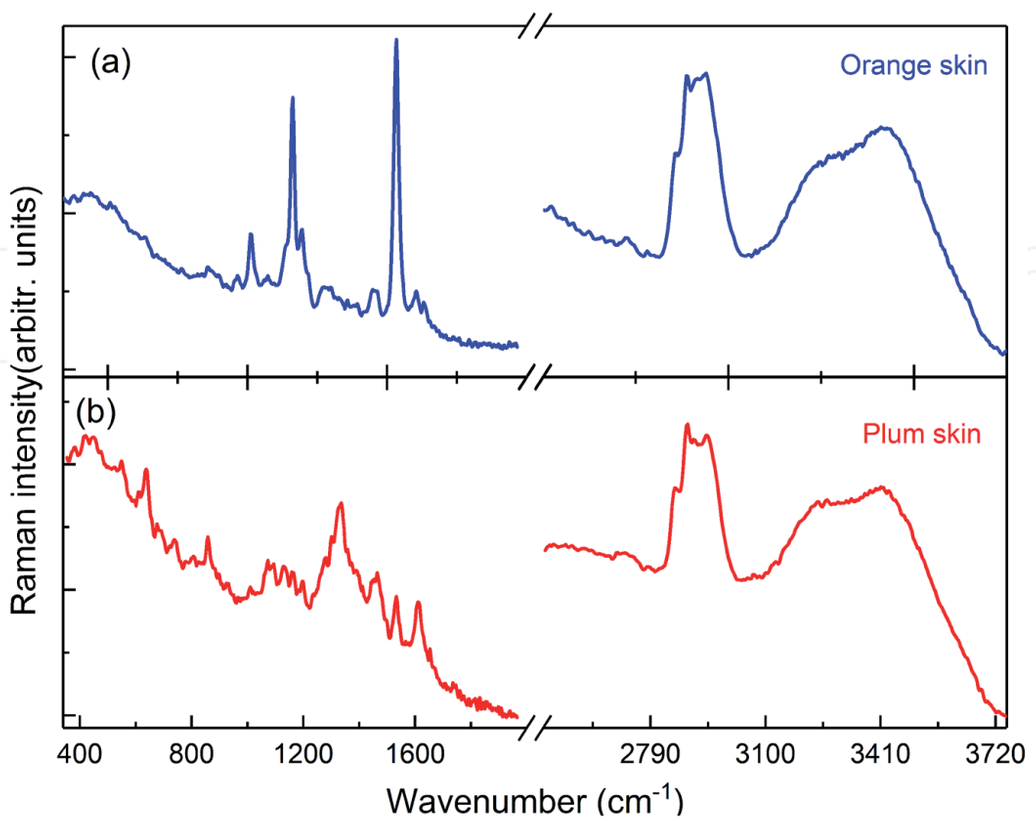

Figure 6.
Raman spectra acquired from skins of orange (a) and plum (b).

that requires NIR laser excitation (e.g., 866 nm). Santos et al. demonstrated acquiring HW Raman signals from pigmented skin lesions with 976 nm excitation [36]. Acquiring the HW Raman signals from orange and plum skins are two other examples of pigmented tissues, [24] as shown in **Figure 6**.

6. Options of InGaAs based Raman spectroscopy for HW signal detection

Based on the InGaAs spectrometer, there are basically three options to set up a Raman spectroscopy to acquire full range Raman spectrum. For a spectrometer that combined an InGaAs detector and a tunable spectrograph, one laser and one spectrometer will allow the acquisition of a full range Raman spectrum that includes the HW region. For a compact InGaAs spectrometer designed to work with a 1064 nm laser, it will typically have a fixed range starting ~1100 and ending ~1350 nm. In order to acquire a full range spectrum, one could add a second laser (e.g., 850 nm) to extend the range to cover the HW region. Alternatively, one could use a single laser (e.g., 850 nm) but use a second spectrometer (e.g., CCD detector based compact spectrometer) to record fingerprint region Raman signals. The advantage of the dual laser plus one spectrometer is it suppress the fluorescence to the maximum extent as 1064 nm is fluorescence free many biological tisses. The disadvantage is that the HW and fingerprint region must be taken consecutively, resulting in different sampling if the specimen is moving or changes with time. While the one laser plus two spectrometers will ensure HW and fingerprint regions are taken simultaneously on a same spot.

Author details

Shan Yang
Department of Chemistry, Physics and Atmospheric Sciences, Jackson State University, Jackson, MS, USA

*Address all correspondence to: Shan.Yang@jsums.edu

References

[1] Banwell, C. N. *Fundamentals of Molecular Spectroscopy*; McGraw-Hill, 1983.

[2] Tsuda, H.; Arends, J. Orientational Micro-Raman Spectroscopy on Hydroxyapatite Single Crystals and Human Enamel Crystallites. J Dent Res 1994, *73* (11), 1703-1710. https://doi.org/10.1177/00220345940730110501.

[3] Penney, C. M.; Goldman, L. M.; Lapp, M. Raman Scattering Cross Sections. Nature Physical Science 1972, *235* (58), 110-112. https://doi.org/10.1038/physci235110b0.

[4] Golcuk, K.; Mandair, G. S.; Callender, A. F.; Sahar, N.; Kohn, D. H.; Morris, M. D. Is Photobleaching Necessary for Raman Imaging of Bone Tissue Using a Green Laser? Biochimica et Biophysica Acta (BBA) - Biomembranes 2006, *1758* (7), 868-873. https://doi.org/10.1016/j.bbamem.2006.02.022.

[5] Movasaghi, Z.; Rehman, S.; Rehman, I. U. Raman Spectroscopy of Biological Tissues. Applied Spectroscopy Reviews 2007, *42* (5), 493-541. https://doi.org/10.1080/05704920701551530.

[6] Bumbrah, G. S.; Sharma, R. M. Raman Spectroscopy – Basic Principle, Instrumentation and Selected Applications for the Characterization of Drugs of Abuse. Egyptian Journal of Forensic Sciences 2016, *6* (3), 209-215. https://doi.org/10.1016/j.ejfs.2015.06.001.

[7] Vandenabeele, P.; Castro, K.; Hargreaves, M.; Moens, L.; Madariaga, J. M.; Edwards, H. G. M. Comparative Study of Mobile Raman Instrumentation for Art Analysis. Analytica Chimica Acta 2007, *588* (1), 108-116. https://doi.org/10.1016/j.aca.2007.01.082.

[8] Chase, B. A New Generation of Raman Instrumentation. *Appl. Spectrosc.,* AS 1994, *48* (7), 14A-19A.

[9] Schrader, B.; Dippel, B.; Erb, I.; Keller, S.; Löchte, T.; Schulz, H.; Tatsch, E.; Wessel, S. NIR Raman Spectroscopy in Medicine and Biology: Results and Aspects. Journal of Molecular Structure 1999, *480-481*, 21-32. https://doi.org/10.1016/S0022-2860(98)00650-4.

[10] Zhang, J.; Li, M.; Feng, Z.; Chen, J.; Li, C. UV Raman Spectroscopic Study on TiO_2. I. Phase Transformation at the Surface and in the Bulk. *J. Phys.* Chem. B 2006, *110* (2), 927-935. https://doi.org/10.1021/jp0552473.

[11] Strom, D.; Breuninger, S.; Fischer, H.; Richter, A.; Schmidt, U.; Hollricher, O. Criteria for High-Quality Raman Microscopy (accessed 2019 -07 -14).

[12] Holst, G. C.; Lomheim, T. S. CMOS/CCD Sensors and Camera Systems, Second Edition | (2011) Spie Press Book.

[13] Nikzad, S.; Hoenk, M. E.; Greer, F.; Jacquot, B.; Monacos, S.; Jones, T. J.; Blacksberg, J.; Hamden, E.; Schiminovich, D.; Martin, C.; Morrissey, P. Delta-Doped Electron-Multiplied CCD with Absolute Quantum Efficiency over 50% in the near to Far Ultraviolet Range for Single Photon Counting Applications. Appl. Opt. 2012, *51* (3), 365. https://doi.org/10.1364/AO.51.000365.

[14] Lesser, M. P. Improving CCD Quantum Efficiency. In *Instrumentation in Astronomy VIII*; International Society for Optics and Photonics, 1994; Vol. 2198, pp. 782-791. https://doi.org/10.1117/12.176777.

[15] Adar, F.; Atzeni, S.; Gilchrist, J. R.; Goldstone, L.; Noonan, J. Detector choice is vital to spectroscopy (accessed 2019 -07 -14).

[16] Hirschfeld, T.; Chase, B. FT-Raman Spectroscopy: Development and

Justification. Appl Spectrosc 1986, *40* (2), 133-137. https://doi.org/10.1366/0003702864509538.

[17] García-Flores, A. F.; Raniero, L.; Canevari, R. A.; Jalkanen, K. J.; Bitar, R. A.; Martinho, H. S.; Martin, A. A. High-Wavenumber FT-Raman Spectroscopy for in Vivo and Ex Vivo Measurements of Breast Cancer. Theor Chem Acc 2011, *130* (4-6), 1231-1238. https://doi.org/10.1007/s00214-011-0925-9.

[18] Church, J. S.; Corino, G. L.; Woodhead, A. L. The Analysis of Merino Wool Cuticle and Cortical Cells by Fourier Transform Raman Spectroscopy. Biopolymers 1997, *42* (1), 7-17. https://doi.org/10.1002/(SICI)1097-0282(199707)42:1<7::AID-BIP2>3.0.CO;2-S.

[19] das Chagas e Silva de Carvalho, L. F.; Sato, É. T.; Almeida, J. D.; da Silva Martinho, H. Diagnosis of Inflammatory Lesions by High-Wavenumber FT-Raman Spectroscopy. Theor Chem Acc 2011, *130* (4-6), 1221-1229. https://doi.org/10.1007/s00214-011-0972-2.

[20] Baraga, J. J.; Feld, M. S.; Rava, R. P. In Situ Optical Histochemistry of Human Artery Using near Infrared Fourier Transform Raman Spectroscopy. PNAS 1992, *89* (8), 3473-3477.

[21] SPECTROSCOPY: Indium gallium arsenide detectors open up the near-IR https://www.laserfocusworld.com/detectors-imaging/article/16555710/spectroscopy-indium-gallium-arsenide-detectors-open-up-the-nearir (accessed 2021 -04 -23).

[22] Unal, M.; Yang, S.; Akkus, O. Molecular Spectroscopic Identification of the Water Compartments in Bone. *Bone* 2014, *67*, 228-236. https://doi.org/10.1016/j.bone.2014.07.021.

[23] He, W.; Livingston, J. C.; Sobiesk, E. R.; Zhou, J.; Zhu, X.; Duan, Y.; Yang, S. A Pilot Study on High Wavenumber Raman Analysis of Human Dental Tissues. J Raman Spectrosc 2020, *51* (4), 630-634. https://doi.org/10.1002/jrs.5812.

[24] He, W.; Li, B.; Yang, S. High-Frequency Raman Analysis in Biological Tissues Using Dual-Wavelength Excitation Raman Spectroscopy. Appl Spectrosc 2020, *74* (2), 241-244. https://doi.org/10.1177/0003702819881762.

[25] Yang, S.; Sen, C.; Thompson, R.; Zhou, J.-G.; Akkus, O. An in Vitro Raman Study on Compositional Correlations of Lipids and Protein with Animal Tissue Hydration. Vibrational Spectroscopy 2020, *107*, 103022. https://doi.org/10.1016/j.vibspec.2020.103022.

[26] Nedić, M.; Wassermann, T. N.; Larsen, R. W.; Suhm, M. A. A Combined Raman- and Infrared Jet Study of Mixed Methanol–Water and Ethanol–Water Clusters. Phys. Chem. Chem. Phys. 2011, *13* (31), 14050. https://doi.org/10.1039/c1cp20182d.

[27] Starciuc, T.; Guinet, Y.; Hedoux, A.; Shalaev, E. Water Content Thresholds in Glycerol/Water System: Low- and High-Wavenumber Raman Spectroscopy Study. Journal of Molecular Liquids 2021, *321*, 114678. https://doi.org/10.1016/j.molliq.2020.114678.

[28] Santos, L. F.; Wolthuis, R.; Koljenović, S.; Almeida, R. M.; Puppels, G. J. Fiber-Optic Probes for in Vivo Raman Spectroscopy in the High-Wavenumber Region. Anal. Chem. 2005, *77* (20), 6747-6752. https://doi.org/10.1021/ac0505730.

[29] Carvalho, L. F. C. S.; Bonnier, F.; Tellez, C.; dos Santos, L.; O'Callaghan, K.; O'Sullivan, J.; Soares, L. E. S.; Flint, S.; Martin, A. A.; Lyng, F. M.; Byrne, H. J. Raman Spectroscopic Analysis of Oral Cells in the High Wavenumber Region. Experimental and Molecular Pathology 2017, *103* (3), 255-262. https://doi.org/10.1016/j.yexmp.2017.11.001.

[30] Barroso, E. M.; Smits, R. W. H.; Bakker Schut, T. C.; ten Hove, I.; Hardillo, J. A.; Wolvius, E. B.; Baatenburg de Jong, R. J.; Koljenović, S.; Puppels, G. J. Discrimination between Oral Cancer and Healthy Tissue Based on Water Content Determined by Raman Spectroscopy. *Anal.* Chem. 2015, *87* (4), 2419-2426. https://doi.org/10.1021/ac504362y.

[31] Caspers, P. J.; Lucassen, G. W.; Bruining, H. A.; Puppels, G. J. Automated Depth-Scanning Confocal Raman Microspectrometer for Rapidin Vivo Determination of Water Concentration Profiles in Human Skin. Journal of Raman Spectroscopy 2000, *31* (8-9), 813-818. https://doi.org/10.1002/1097-4555(200008/09)31:8/9<813::AID-JRS573>3.0.CO;2-7.

[32] Caspers, P. J.; Bruining, H. A.; Puppels, G. J.; Lucassen, G. W.; Carter, E. A. In Vivo Confocal Raman Microspectroscopy of the Skin: Noninvasive Determination of Molecular Concentration Profiles. Journal of Investigative Dermatology 2001, *116* (3), 434-442. https://doi.org/10.1046/j.1523-1747.2001.01258.x.

[33] Choe, C.; Lademann, J.; Darvin, M. E. A Depth-Dependent Profile of the Lipid Conformation and Lateral Packing Order of the Stratum Corneum in Vivo Measured Using Raman Microscopy. The Analyst 2016, *141* (6), 1981-1987. https://doi.org/10.1039/C5AN02373D.

[34] Quatela, A.; Miloudi, L.; Tfayli, A.; Baillet-Guffroy, A. In Vivo Raman Microspectroscopy: Intra- and Intersubject Variability of Stratum Corneum Spectral Markers. Skin Pharmacology and Physiology 2016, *29* (2), 102-109. https://doi.org/10.1159/000445079.

[35] Lauritsen, A. K.; Pereira, J. E. M.; Juranyi, F.; Bordallo, H. N.; Larsen, L.; Benetti, A. R. Probing Water Mobility in Human Dentine with Neutron Spectroscopy. J Dent Res 2018, *97* (9), 1017-1022. https://doi.org/10.1177/0022034518763051.

[36] P. Santos, I.; van Doorn, R.; Caspers, P. J.; Bakker Schut, T. C.; Barroso, E. M.; Nijsten, T. E. C.; Noordhoek Hegt, V.; Koljenović, S.; Puppels, G. J. Improving Clinical Diagnosis of Early-Stage Cutaneous Melanoma Based on Raman Spectroscopy. *Br J Cancer.* 2018, *119* (11), 1339-1346. https://doi.org/10.1038/s41416-018-0257-9.